ELSEVIER

Cement & Concrete Composites 23 (2001) 157–169

Cement & Concrete Composites

www.elsevier.com/locate/cemconcomp

Some fields of applications of automatic image analysis in civil engineering

Jean-Louis Chermant *, Liliane Chermant, Michel Coster, Anne-Sophie Dequiedt, Carl Redon [1]

LERMAT, URA CNRS 1317, ISMRA, 6 Bd Maréchal Juin, 14050 Caen Cedex, France

Abstract

This paper illustrates the use of automatic image analysis technique to investigate the morphology of cement, concrete and fibre-reinforced concrete. First the methods to be used for powders and secondly for mortar and concrete are introduced. The dispersed phases are characterized by classical morphological parameters: these also enable to accede to the hydration process. The covariances give quantitative information on the homogeneity and dispersion of the different components: gravel, air-voids and cement paste. Air-voids are characterized by granulometric distributions and their mean free paths. Rose of directions gives information on feature orientation: fibres, microcracks for fibre-reinforced concrete, etc. Finally probabilistic models can be used to simulate the microstructure of such materials.

Keywords: Automatic image analysis; Cement; Mortar; Fibre-reinforced concrete (FRC); Stereological parameters; Dispersion; Homogeneity; Granulometry; Air-void distances; Orientation; Simulation

1. Introduction

For a long time morphology of cement, mortar and concrete has been considered to play an important role on their mechanical properties, freeze-thaw resistance, etc., [1–4]. To increase these characteristics requires a control of their morphology and homogeneity.

Former studies have shown the interest of the methods based on image analysis [5–11]. But most often they were developed manually or semi-automatically using, for example, a digitizing table. But in this way they do not permit a complete morphological description. Moreover if one wants to describe statistically the morphology of these materials, automatic image analysis and processing allow to solve this problem [12].

The objective of this paper is to give briefly some examples to illustrate the use of automatic image analysis techniques to measure some morphological characteristics of cement, concrete and fibre-reinforced concrete (FRC). The image analysis methods used will not be really detailed: they are recalled in the first paper of this special issue [13]. They are always based on classical methods described previously [14–17].

2. Cement powders

As particulate cement is obtained by grinding clinker, gypsum and different additives, any morphological information will be obtained from projected images of powders.

2.1. Cement powder

Due to chemical complexity of the cement powder, the only morphological investigation to be considered is the size distribution studies with a possible extension to shape studies. For such purpose the powder must be dispersed on a support taking care that each ''grain'' will be separated from its neighbours. To avoid the presence of agglomerate is, in practice, very difficult. When SEM observations are made, in order to have a correct contrast between the cement and support one must choose an appropriate support to facilitate the threshold step.

* Corresponding author. Tel.: +33-231-452-664; fax: +33-231-452-660.

[1] Present address: Saint Gobain, Matériaux de Construction International, 39 quai Lucien Lefranc, 93303 Aubervilliers, France.

0958-9465/01/$ - see front matter
PII: S0958-9465(00)00059-7

By individual analysis many size criteria [18] can be used, such as surface area, perimeter, Feret diameters (the greatest and the smallest dimension in a given direction), etc. The combination of these parameters can give shape index [17,19], such as lengthening index ($\mathrm{Feret_{min}}/\mathrm{Feret_{Max}}$), concavity index, etc.

Nevertheless a valid analysis requires the measurement of many grains (1500–2000 is a minimum) that can be time-consuming, compared to the use of physical methods, such as laser granulometry or sedimentation methods. These latter methods are unable to give information on the shape and cannot be used correctly if the particle size is smaller than the wavelength of the laser beam, despite Mie's theory in the case of laser granulometry.

2.2. Cement clinker

To improve the clinker process, morphology of the different components of the clinker can be characterized. As the clinker is crumbly and brittle, it must be impregnated, under vacuum, by a resin before the grinding and polishing steps. A chemical etching will facilitate the phase differentiation.

Although many qualitative investigations have been published [20], only a few concern quantitative studies due to the complex microstructure of the clinker. Nevertheless one can quote the work of Roux [21–23] where an image analysis method has been developed to identify and quantify the different clinker phases. Complex procedures were developed: they are based on a segmentation procedure from the local histograms [24], an algorithmic processing of the images [25] and an automatic threshold [26]. To improve segmentation of the different phases, many morphological tools (closing, erosion-reconstruction, etc.) were used [16,17].

3. Mortar and concrete

On mortar and concrete one can investigate the morphology of its phases, their dispersion, homogeneity of the materials, the air-void distances, the hydration process, the microcrack orientation, etc. Some of these morphological aspects will be presented here.

3.1. Morphological parameters: morphology of the dispersed phases

Among the different morphological and stereological parameters [they are defined in [14–17] the most useful can be the volume fraction of a phase, $V_V(X)$, its specific surface area, $S_V(X)$, its integral of mean curvature per unit volume, $M_V(X)$, its surface area fraction, $A_A(X)$, its number of connectivity per unit surface, $N_A(X)$, and also the mean free path in a given phase in $\mathbb{R}^1, L_1(X)$, the mean surface area in $\mathbb{R}^2$, $\overline{A}(X)$, and the mean curvature in $\mathbb{R}^3, \overline{H}_3(X)$.

Fig. 1 presents the evolution of the specific surface area of the volume fraction of the anhydrous phase (NH), S_V(NH), as a function of the volume fraction of the anhydrous phase, V_V(NH) for two cements with a water/cement ratio, w/c, of 0.3 and 0.5 [27,28]. The same type of curve is obtained for other morphological parameters such as H_3(NH), [29]. Such evolution informs on the influence of the w/c ratio. A value of 0.42 corresponds to the full hydration of cement, as it has been shown by Dupain et al. [30]. The change in S_V(NH) appears more or less pronounced if w/c is below or above the 0.42 value due to the chemical reactions on the surface of particles. For a value of 0.3, the material contains more anhydrous grains per unit surface than for a material with a value of 0.5. Moreover, the anhydrous grains are larger for materials with w/c = 0.3 than with 0.5.

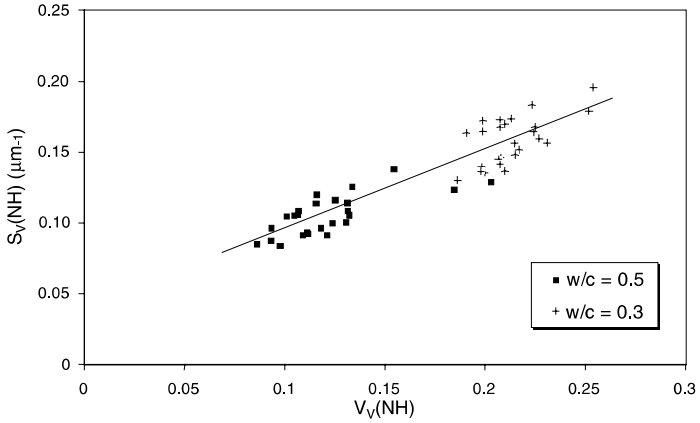

Fig. 1. Change in the specific surface area, S_V(NH), as a function of the volume fraction of the anhydrous phase, V_V(NH), for different cements with a water/cement ratio of 0.3 and 0.5.

The knowledge of the fraction of air-voids and their number per unit surface area (Fig. 2), respectively, A_A(air-voids) and N_A(air-voids), allows to illustrate and better understand the role of the morphology of air-voids on the compressive strength of an ordinary cement (m) and the same cement reinforced by metallic glass ribbons (f), (Fig. 2), [6,31,32]. In this as formulated FRC, the maximum strength values correspond to an optimum superplasticizer content close to $s = 0.5\%$ (superplasticizer dry content related to the cement mass). For this value the number of air-voids per unit surface has been found to be the smallest, after which there is an increase in a larger amount of the superplasticizer, s. The lower the N_A values so long as A_A equally goes down, the better the compressive strength, the better the compactness. One also notes that the fraction of air-voids for the same concrete but reinforced by ribbons is a bit higher than for an ordinary concrete, but globally the number of air-voids per unit surface in this ordinary concrete is larger than in those reinforced ones. So the mechanical strength evolution can be explained from a correct knowledge of some

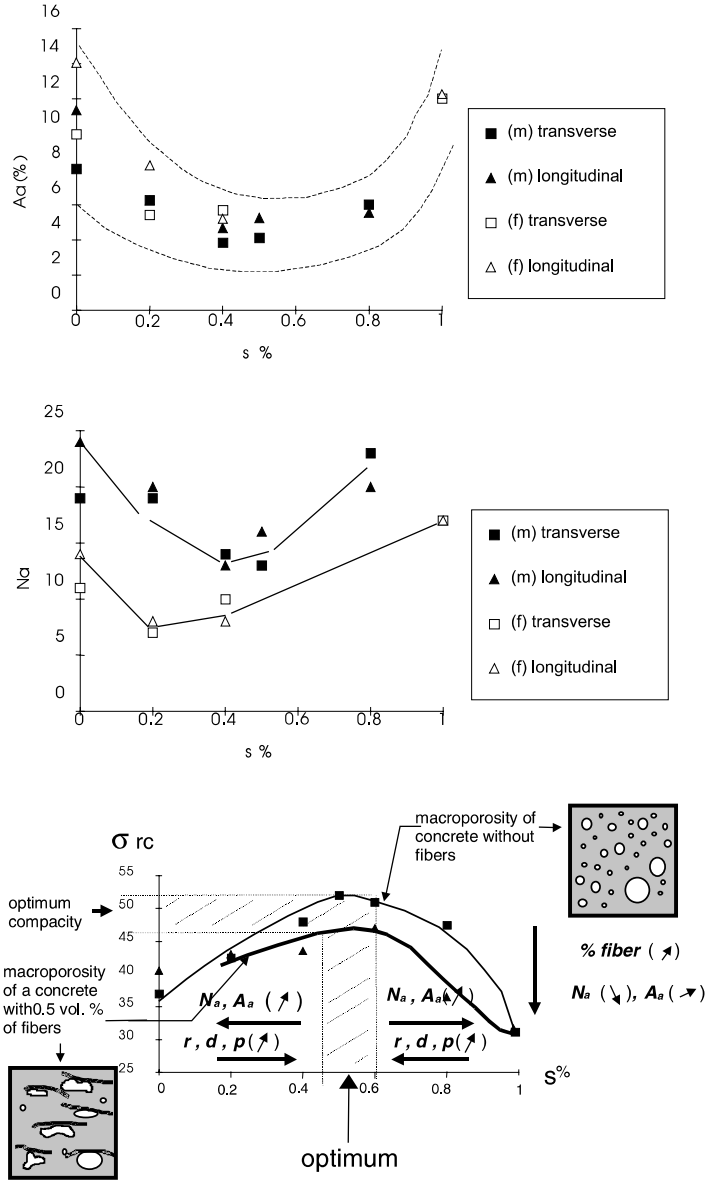

Fig. 2. Change in the surface area and number of air-voids (larger than 200 μm in diameter), respectively, A_A and N_A, and in the compressive strength, σ_{rc}, as a function of the superplasticizer content, s, for ordinary, m, and reinforced, f, concrete. r, d and p correspond to three different parameters related to the air-void distances. Automatic image analysis was conducted on 27 (3×3 cm^2) longitudinal and 27 transversal observation fields, for each superplasticizer content, in the case of an ordinary concrete (m), as well as in the case of a reinforced concrete (f). Longitudinal and transverse sections of the specimens correspond to their orientation with regard to the casting axis, respectively, perpendicular and parallel.

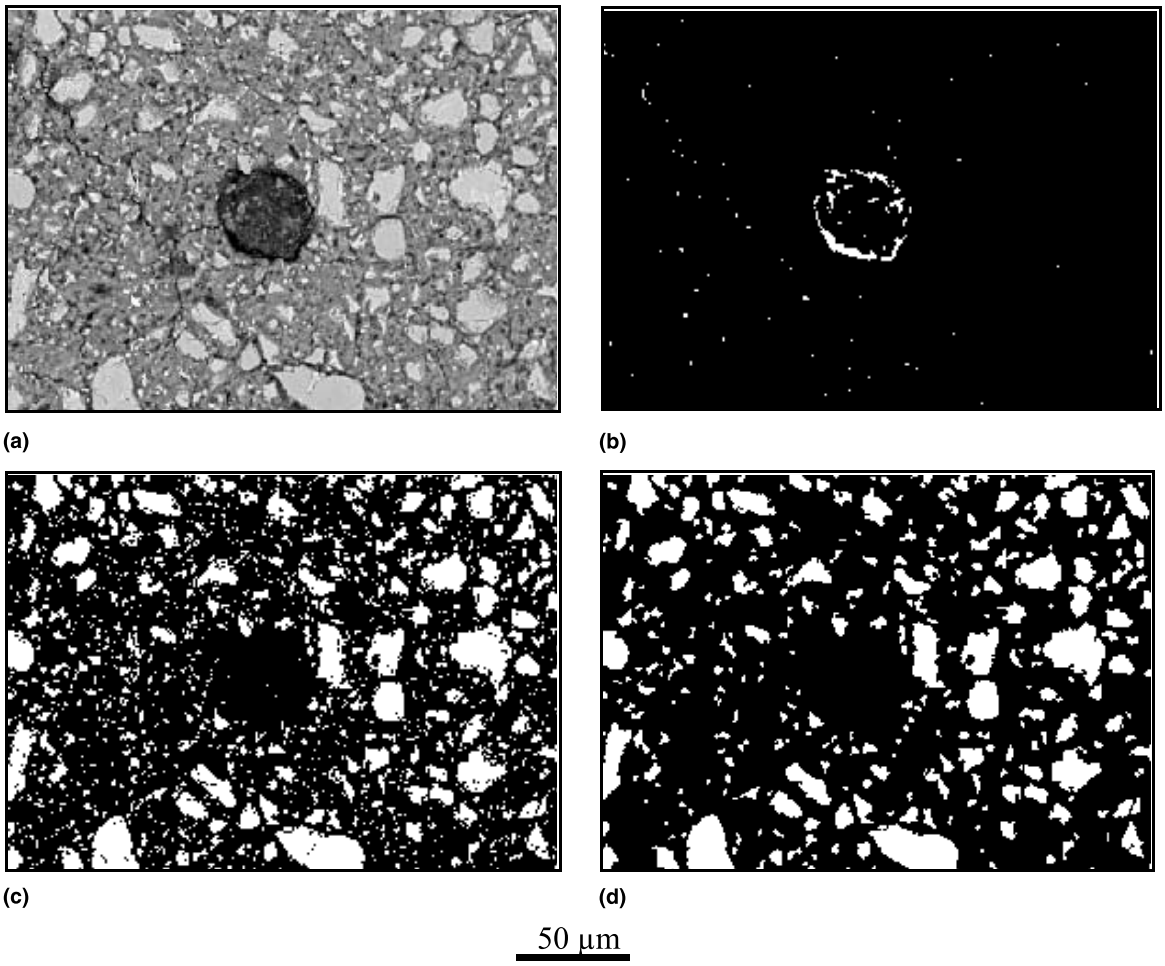

Fig. 3. (a) SEM image in backscattered electron mode of cement with a pore; (b) image after a threshold by maximum contrast; (c) thresholded image; (d) final image.

morphological parameters directly related, in that example, to air-voids. In this case an usual global porosity measurement would not have given any information on the presence of large-shaped air-voids responsible for the low compactness (density) of the (m) concrete.

3.2. Morphological parameters: hydration process

If now the variation of similar morphological parameters is plotted as a function of time, t, one can get access to information on the hydration process [27,28,33].

As by scanning electron microscopy it is possible to distinguish, by backscattered electron mode, clear zones corresponding to anhydrous phases (NH) from dark ones corresponding to hydrated (H) ones, one can follow by automatic image analysis the degree of hydration, α_{AIA}. It can be estimated from the volume fraction of the anhydrous phase, $V_V(NH)$. This 3D parameter is equal to the surface fraction, $A_A(NH)$, measurable in 2D by image analysis [34]. The degree of hydration, α, is calculated from:

$$\alpha = 1 - \frac{\text{weight of non-hydrated cement}}{\text{initial weight of anhydrous cement}} = 1 - \frac{P_{\text{anhydrous cement}} \cdot A_A(NH) \cdot V_{\text{specimen}}}{\text{initial weight of anhydrous cement}},$$

where $P_{\text{anhydrouscement}}$ is the volume weight of anhydrous cement, $A_A(NH)$ the surface fraction of anhydrous phase on the images of the cement paste and V_{specimen} is the volume of the specimen.

Then automatic treatment can be easily performed by filtering, threshold and the use of a binary treatment based on an opening-reconstruction (these terminologies are defined in [13,16,28]). Fig. 3 presents the process sequence.

Some morphological evolutions are presented in Fig. 4, corresponding to the degree of hydration, α_{AIA}, the specific surface area of the anhydrous phase,

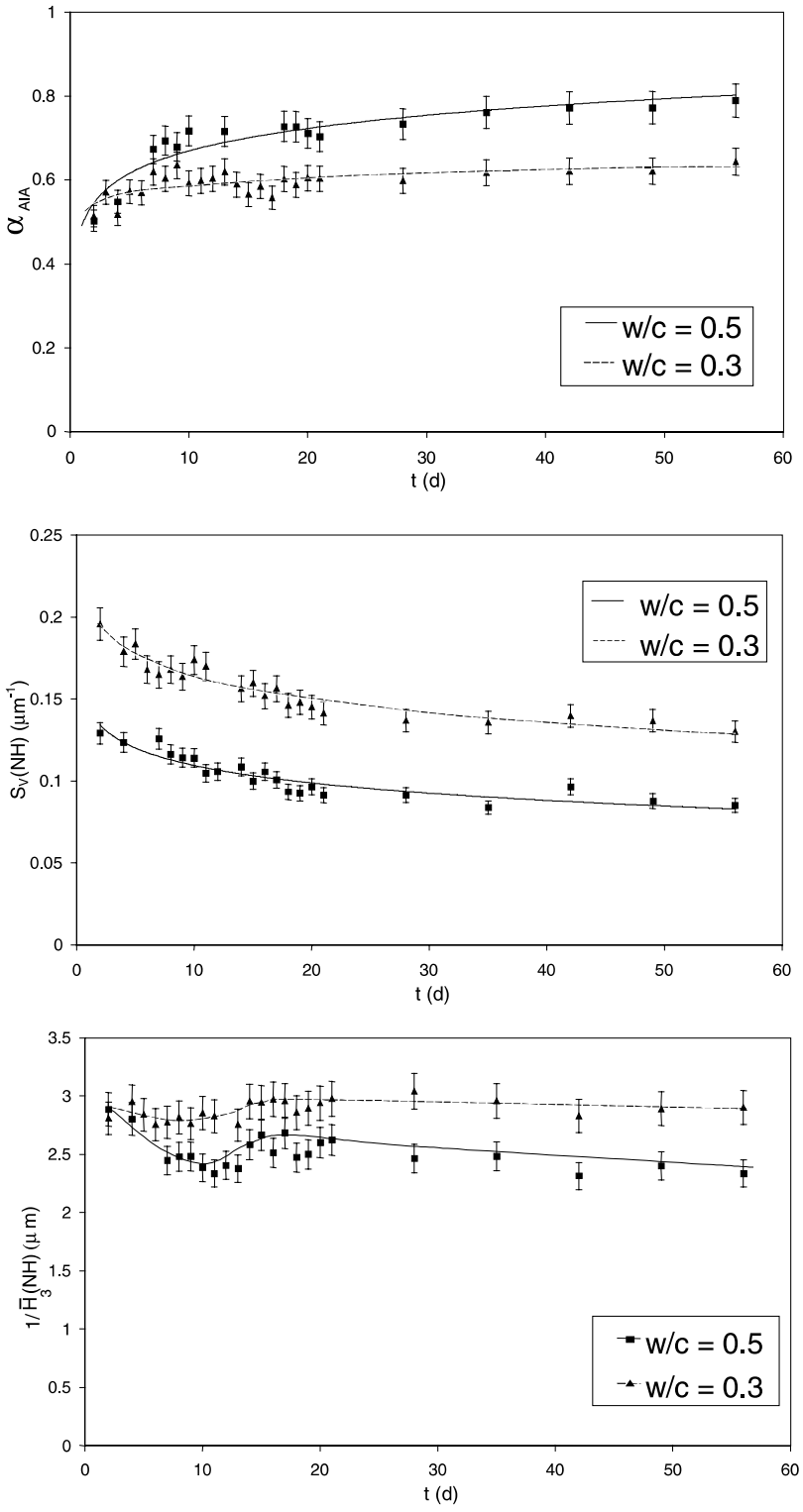

Fig. 4. Change in the degree of hydration, α_{AIA}, the specific surface area of the anhydrous phase, $S_V(NH)$, and the reciprocal mean curvature of the anhydrous phase in $\mathbb{R}^3$, $1/\overline{H}_3(NH)$, as a function of time, t (in days), for two cements with w/c = 0.3 and 0.5.

$S_V(NH)$, and of the reciprocal mean curvature of the anhydrous phase in $\mathbb{R}^3$, $1/\overline{H}_3(NH)$, as a function of time, t, for two cements with w/c = 0.3 and 0.5, [27,28].

After two days for a cement with w/c = 0.3, the hydration increases slowly, while for a cement with w/c = 0.5 it increases significantly between 2 and 15 days

and then reaches an asymptotic value (about 0.80). Such evolutions agree with classical investigations already published on the kinetics of hydration of a cement [35]. The w/c has limited influence on the rate of hydration during the first days. But later on, the lower the w/c, the lower the hydration rate. Of course other parameters also have influence, such as temperature, chemical composition, etc.

The change in the mean curvature in $\mathbb{R}^3$ shows that the anhydrous phase reaches rapidly a constant curvature (which is the reciprocal of the curvature radius) after seven days. The low increase of this parameter during the first days corresponds to the disappearance of the smallest anhydrous grains. This was also confirmed by the change in the mean chord length (i.e. the mean length of an object intersected by a straight line), $\overline{L}_1(\mathrm{NH})$, [28]. It shows that morphological parameters linked to curvatures are important to correctly follow the change in the evolution of the microstructure during the hardening process. Moreover the change in the specific surface area of the anhydrous phase can be interpreted from the energy of the system: during the first days, there is a minimization of the superficial energy between phases, then the interfacial parameter takes a stationary value. The decrease of $S_V(\mathrm{NH})$ confirms the free energy of the system by minimization of the interfacial energy which tends to stabilize.

3.3. Dispersion and homogeneity: morphology of the matrix

As it has been recalled [13] the dispersion of a phase in a matrix can be quantified using either a distance function or the distribution of the nearest neighbours [29]. The covariance function, $C(X,h)$, appears to be a suited tool, as it informs on the dispersion and homogeneity [16,17]. One has used either the simple covariance for air-voids and gravel, and the crossed-covariance for air-voids and matrix, gravel and matrix, and air-voids and gravel, [27,29].

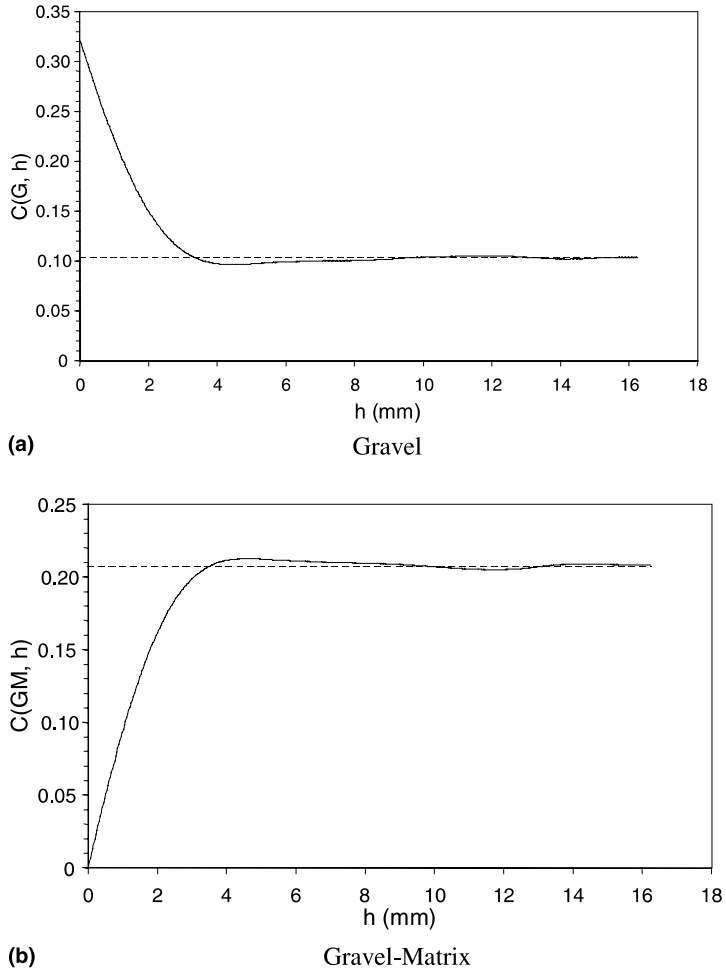

Fig. 5. Covariance curves of gravel, $C(G,H)$, (a), and crossed-covariance of gravel–matrix, $C(GM,h)$, (b), for a concrete without air entraining additive.

Fig. 5 presents a typical covariance curve of gravel for a concrete without air entraining additive, $C(G,h)$, and a crossed-covariance curve for gravel and matrix, $C(GM,h)$, for the same concrete. Such curves indicate that a minimum distance of 3 mm is necessary to analyse to have a correct representativity of an experimental parameter [27]. From any observation of concrete one notes large areas of matrix with pores between gravel as there is generally few gravel. The crossed-covariance is the result of an intersection of one phase with another one of the initial image: it informs on the correct dispersion of gravel in the matrix for a batch of concrete. As the pores are in contact with the matrix, the asymptote of the covariance plot is rapidly reached as there is no obstruction by the gravel.

The same result is obtained for the gravel/matrix phases, as the pores are very small compared to gravel. That is the reason why the plateau is rapidly reached. The slope at the origin gives the specific surface area of contact between gravel and matrix, $S_V(GM)$. The experimental value obtained (0.42) is rigorously equal to the total specific surface area of the gravel, $S_V(G)$, determined from the stereological parameters and the simple covariance on gravel. It confirms that gravel is only surrounded by the matrix and that there are no air-voids in contact with gravel. Such an information is very important, especially if one wishes to model the microstructure of such materials [36].

As it will be also shown in this issue [29], the co-occurrence matrices give access to the dispersion homogeneity of the fraction of surface area on the 16-grey levels.

3.4. Granulometry of air-void distances: morphology of voids

Air-voids generally induce strength loss, it can give access to the water, and consequently diminishes strongly the freeze-thaw resistance [37–39]. Thus it is of importance to know their size and spatial distribution within the hardened concrete.

By individual analysis one can obtain the size distribution of air-voids, and consequently their mean size and standard deviation. But the main difficulty is to choose a correct magnification which does not give a bias to the size distribution (eliminating too much small air-voids and the largest ones if they cut the frame of measurements). Fig. 6 shows an example of such a curve. One notes that this curve is spread out and that the standard deviation, $\overline{\sigma}$, is higher than the mean value, $\overline{D}$. Nevertheless 95% of the observed air-voids have a diameter between 10 and 200 μm: $\overline{D}_V = 86.5$ μm with $\overline{\sigma} = 94.7$ μm.

With regard to the measurements of distances between air-voids, there are many ways to perform them.

Several approaches were investigated in our laboratory [27,31,40–43] regarding the distances between air-voids: (1) the distribution of distances, d, between two voids' nearest neighbours, (2) the distances, p, between all neighbours which correspond to the use of the skeleton by the influence zone (SKIZ) method, and the (3) map-making of distances, r, between one point of the concrete to a void [44]. These methods were used in the euclidean and geodesic spaces. Fig. 7 illustrates the results obtained by the SKIZ method for a hardened cement paste [27,43]. One notes that the geodesic mean distances are always greater than

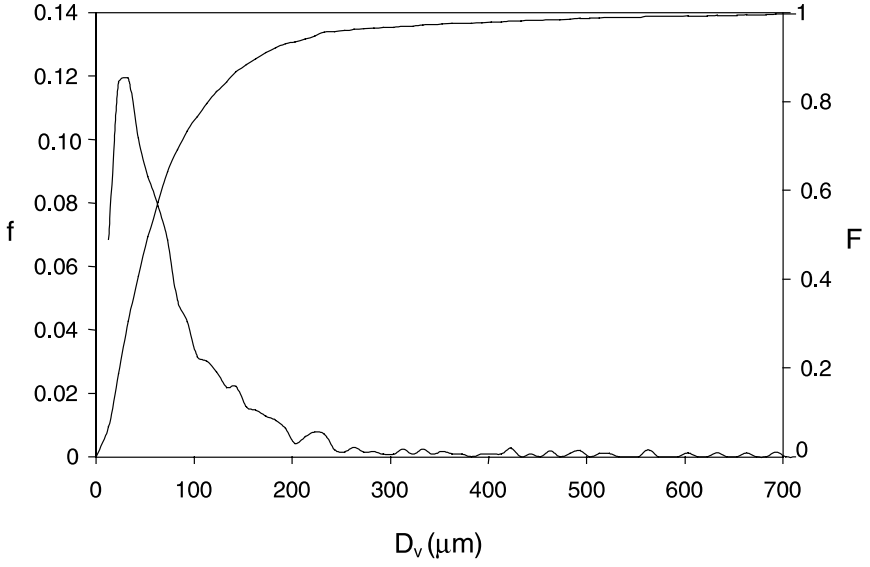

Fig. 6. Granulometric density, f, and cumulated distribution, F, of air-voids, D_V, by individual analysis.

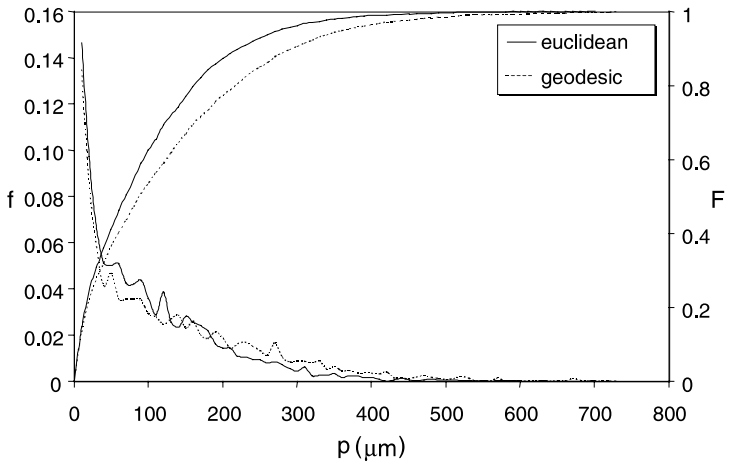

Fig. 7. Distribution (granulometric density, f, and cumulated distribution, F) of the distances, p, between air-voids, according to the SKIZ method.

the euclidean ones. However the distributions stay similar: their reduced quartiles and standard deviations are identical. So such methods bring a statistical aspect and a reproducibility for the measurement of such distances, which are classically measured by manual methods. Moreover there is now a panel of air-void distance parameters available to correlate with the freeze-thaw resistance.

Regarding air-voids it is also possible to reach other information, such as the number of air-voids per size classes or the surface occupied by the air-voids as a function of their size [27,40].

3.5. Microcrack orientation: morphology of damages

When a cement or a concrete is loaded (in tension or in compression) many microcracks result after the elastic strain domain [10,11,45–47]. The morphological knowledge helps to understand their mechanical behaviour and to develop mechanical models [31,48]. A correct quantification of these microcracks can be possible, such as their length, number, mean free path and their orientation.

If the first three parameters are obvious (easy) to measure (when the problem of magnification is chosen), the orientation of the microcracks requires the use of specific methods. One can use the rose of intercepts (where the number of intercepts in a given direction is measured [15,17]). But when there are more than two main orientations, it is better to use the rose of directions (where the length of microcracks in a given direction is measured [15,17]). The orientation can also be investigated via the Fourier transform [49].

An example will be given in the next section, concerning the fibre-reinforced concrete.

4. Fibre-reinforced concrete

The morphology of fibre-reinforced concrete, FRC, can be quantified from all the morphological parameters previously described for mortar and concrete. But in addition one can define the morphological characteristics of the fibres.

4.1. Fibre orientation: morphology of fibres

The determination of the fibre orientation in an FRC is an important knowledge if one wants to check its isotropy and verify if it can or not be loaded evenly in any direction. Indeed an anisotropic fibre orientation may induce, or reciprocally delay, microcrack damage growth along specific axes of the structure.

One has used the Fourier transform [49] on X-ray photographs on a concrete reinforced by amorphous cast iron ribbons (from SEVA, Pont à Mousson, France), [31]. The advantages of this method are to promote a rapid global estimate of orientation, to be less sensitive to the digitizing artefacts induced by the discretized grid of the analyser [50], and, moreover, quite narrow angular sectors can be investigated. Fig. 8 shows the fibre orientation in transverse and longitudinal sections. One notes that the fibre orientation is approximately anisotropic in the 2D projected images of this particular FRC in sections which are parallel to the casting axis [31,49]. Such information is important with regard to mechanical characteristics.

These results are in agreement with the works of Debicki [51] dealing with orientation measurements performed by the total projection methods [8] on a similar material. So there is an effect of the casting direction on the morphology (architecture) of the as-made

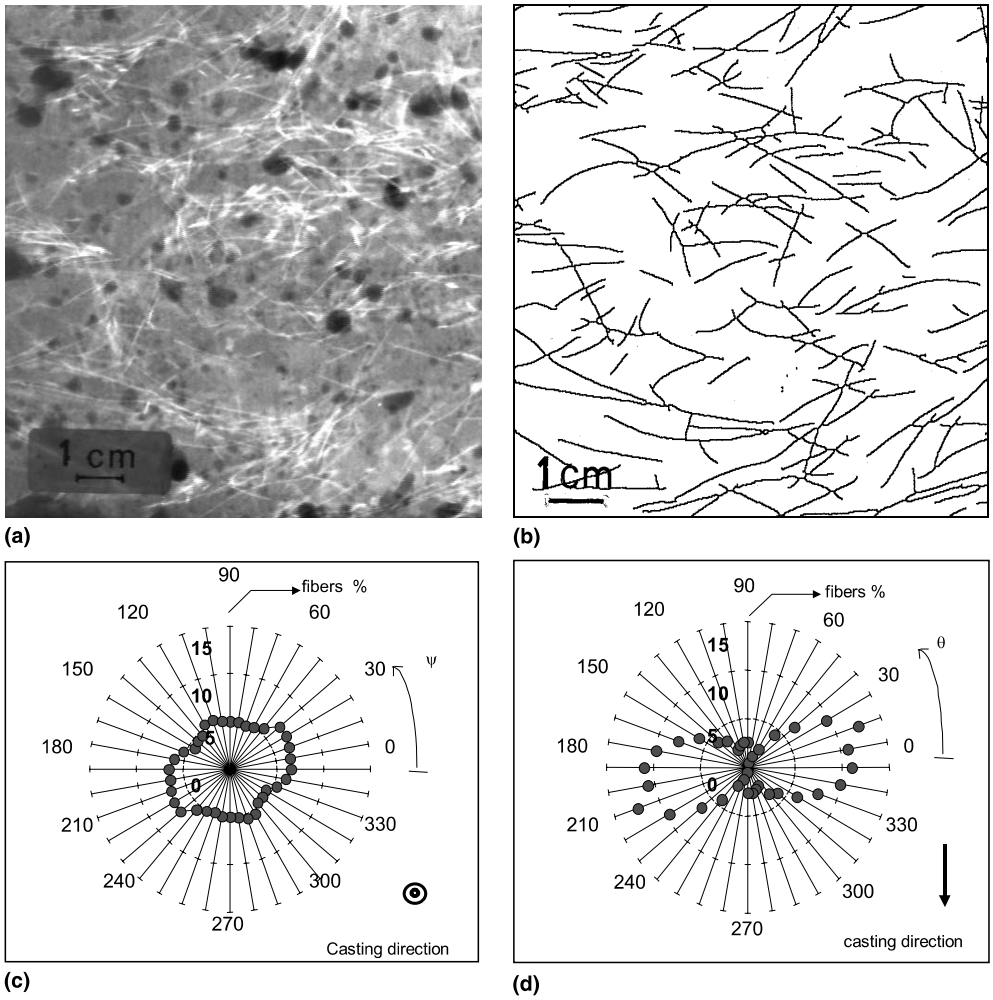

Fig. 8. (a) X-ray image of a transverse section of 10×10 cm^2 of an FRC; (b) digital image of the fibres; (c) roses of fibre directions in sections perpendicular and (d) parallel to the casting axis.

structure. This information will be of interest to the mechanical engineers, as it will be seen in the next paragraph.

4.2. Microcrack orientation: morphology of damages

As for cement and concrete, one can characterize the microcrack orientation. Such an investigation was undertaken in the case of FRC cylinders ($\varnothing = 16.3$ cm, $h = 32$ cm) loaded in uniaxial compression. The concrete was reinforced with amorphous cast iron ribbons (already described). Fig. 9 presents the results. One notes that microcracks are rather oriented in the 90° direction for loaded material than in the 0°–180° one for the unloaded material. Moreover the microcrack lengths increase in the ±90° direction with the strain level. As it corresponds to the direction parallel to the loading axis, it means that the fibres must be oriented perpendicular to the compression axis in order to block the microcrack propagation. Such information is of importance to civil engineers when they want to choose a model of mechanical behaviour [48].

5. Simulation of concrete and fibre-reinforced concrete

As topological parameters in $\mathbb{R}^3$, the state of phase dispersion, etc., are not accessible from measurements in $\mathbb{R}^3$, so stereology is often inefficient to estimate 3D morphological parameters. Probabilistic models are an elegant solution to solve this difficulty [52,53]. They allow, for example, access to the number of particles per unit volume, without any hypothesis and without using serial sections. So it could be interesting to simulate the morphology of a concrete, as it can also avoid to undertake some experiments on such materials which are very time consuming. The best methods, which give results very close to real microstructures, are based on

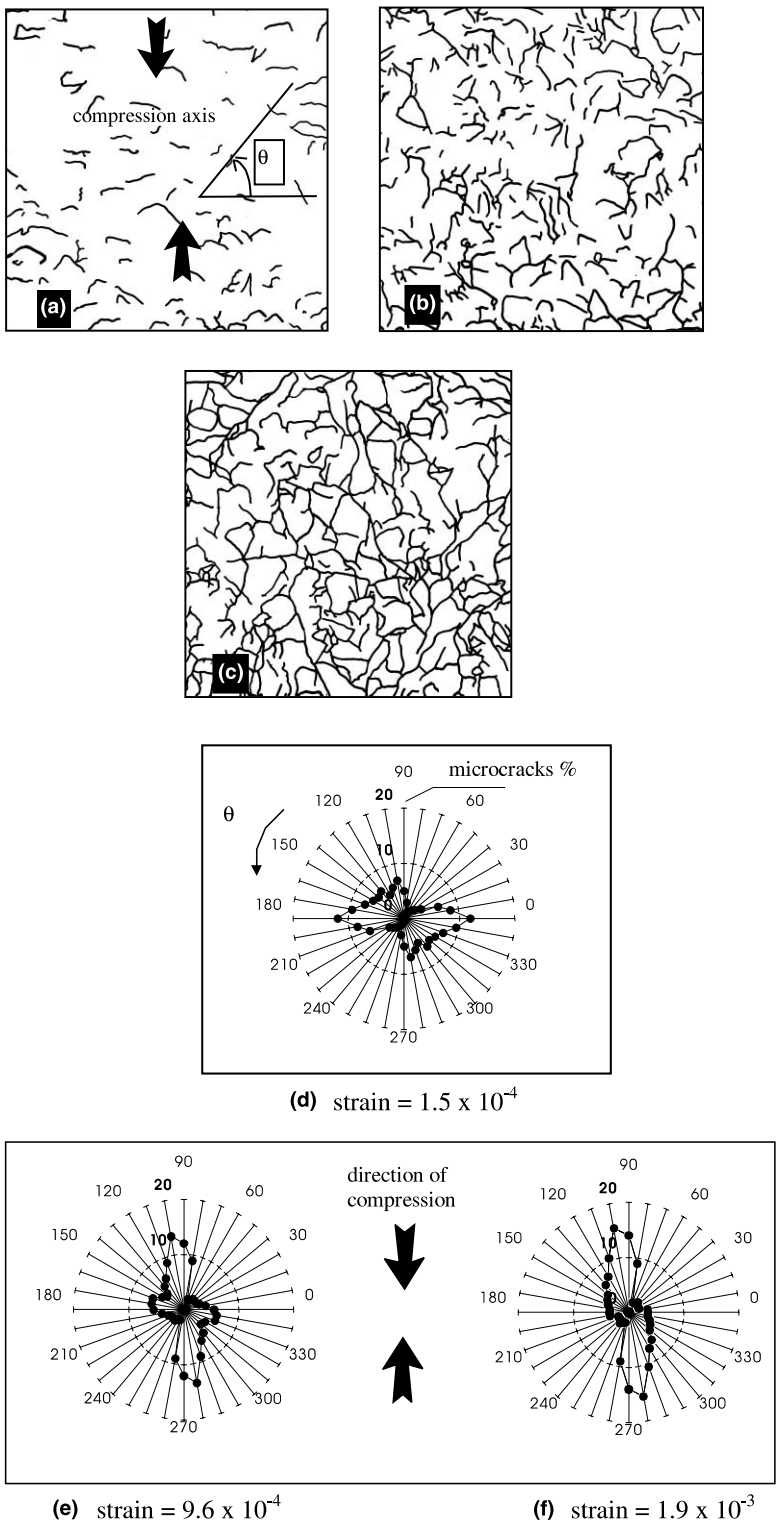

Fig. 9. Microcrack patterns observed for increasing axial compression strains, ε, during compression tests of a fibre reinforced concrete: (a) $\varepsilon = 1.5 \times 10^{-4}$; (b) $\varepsilon = 9.6 \times 10^{-4}$; (c) $\varepsilon = 1.9 \times 10^{-3}$ (the visualized sections on that figure correspond to 100×100 mm^2). Corresponding roses of directions of the microcracks, θ, in longitudinal sections as a function of the increasing compression strain, ε, (d, e, f).

probabilistic models such as Boolean schemes and on Voronoi partitions [52–55]. Other ones can be based, for example, on discrete numerical modelling [56].

The simulation, in $\mathbb{R}^2$, of a concrete can be obtained from [27,36]: first, the modelling of the gravel from a Voronoi partition (followed by different morphological

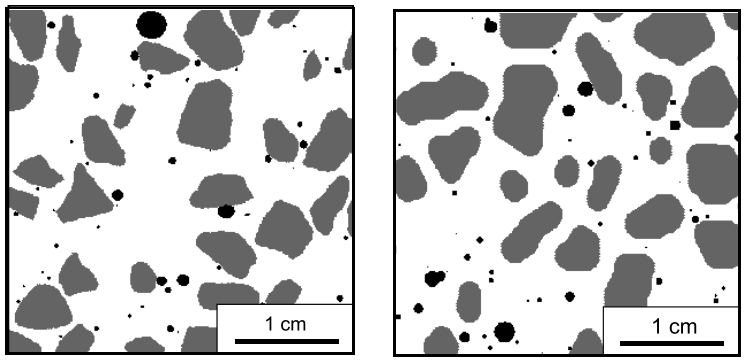

Fig. 10. Simulation of a concrete in 2D: (a) true microstructure; (b) simulated image.

operations), followed, secondly, by the modelling of the voids carried out from a Boolean scheme of spherical primary grains implemented with an exponential distribution law and by eliminating the pores/gravel intersections, as it has been shown by Dequiedt [27]; so by union one obtains the simulated microstructure (Fig. 10(b)) which is very close to a true 2D microstructure (Fig. 10(a)). The covariance obtained on the true microstructures and the simulations are very similar [36].

In the case of FRC such probabilistic models can also be used, but in addition in using now a simulation with three components [57].

6. Conclusion

In this paper many illustrations are given of the use of automatic image analysis methods in order to quantify the morphology of cement powder and clinker, the morphology of the dispersed phases, of the matrix, of the air-voids, of the microcracks in concrete, of the fibres in FRC, and to quantify the evolution of the hydration process.

The results presented are not always new ones, some were already obtained by manual or semi-automatic methods a long time ago by other authors. But, here, all the presented results were performed automatically by image analysis techniques, which means that they were obtained in a statistically and repeatable manner. Moreover homogeneity and dispersion can only be statistically measured from the covariance functions, which can only be performed by automatic technique.

Automatic image analysis appears as a suitable tool to access to many morphological parameters. That should allow to establish a better understanding between morphological parameters and the process or/and physical properties of such civil engineering materials.

Acknowledgements

This work has been performed in the framework of the "Pôle Traitement et Analyse d'Images" de Basse-Normandie (Pôle TAI): Image Processing and Analysis Pole of Basse-Normandie. We wish to thank the Région de Basse-Normandie and ESTP d'Epron for the fellowship (CR), the Ministère de l'Education Nationale, de la Recherche et de la Technologie (MENRT) also for the fellowship (ASD), and ESITC, Groupe ESTP Caen, for the use of their equipments.

References

[1] Moranville-Regourd M. Microstructure of high performance concrete. In: Malier Y, editor. High performance concrete from material to structure. London: E & FN Spon; 1992. p. 3–33.
[2] Lewis JA, Kriven WM. Microstructure-property relationships in macro-defect-free cement. Mat Res Soc Bull 1993;18:72–7.
[3] Brandt AM. Cement-based composites, materials, mechanical properties and performances. London: E & FN Spon, Chapman and Hall; 1995.
[4] Jaiswall SS, Igusa T, Styer T, Karr A, Shah SP. Influence of microstructure and fracture on the transport properties in cement-based materials. In: Brandt AM, Li VC, Marshall ICH, editors. Proceedings of the International Symposium on Brittle Matrix Composites, BMC5, Warsaw, 13–15 October 1997. Warsaw: BIGRAF and Woodhead Publishers; 1997. p.199–220.
[5] Stroeven P. Some aspects of the micromechanics of concrete. PhD Thesis, TU Delft University of Technology, The Netherlands, 1973.
[6] Chatterji S, Gudmundsson H. Characterization of entrained air bubble systems in concrete by means of an image analysing microscope. Cement Concr Res 1977;7:423–8.
[7] Kasperkiewicz J, Malmberg B, Skarendahl A. Determination of fibre content, distribution and orientation in steel fibre concrete by X-ray technique. In: Proceedings of the RILEM Symposium on Testing and Test Methods of Fibre Cement Composites, Sheffield, UK. Lancaster: The Construction Press; 1978. p. 297–314.
[8] Stroeven P. Stereology of concrete reinforced with short steel fibres. Fract Mech Struct Aspects Concr 1986;31:15–28.

[9] Stroeven P. Stereological approaches to cementitious composites. In: Kato Y, Takaki R, Toriwaki, editors. Proceedings of the First Internatioinal Symposium for Science on Form. Tokyo: KTK Scientific Publishers; 1986. p. 175–82.
[10] Ringot E. Automatic quantification of microcrack network by stereological method of total projection in motars and concretes. Cement Concr Res 1988;18:35–43.
[11] Stang H, Mobasher B, Shah SP. Quantitative damage characterization in polypropylene fibre reinforced concrete. Cement Concr Res 1990;20:540–58.
[12] Redon C, Chermant L, Chermant JL, Coster M. Automatic image analysis and morphology of fiber reinforced concrete. Cement Concr Comp 1999;21:403–12.
[13] Coster M, Chermant JL. Image analysis and mathematical morphology for civil engineering materials. Cement Concr Comp 2001;23:133–51.
[14] De Hoff RT, Rhines FN. Quantitative microscopy. New York: McGraw-Hill; 1968.
[15] Underwood EE. Quantitative stereology. Reading, MA: Addison-Wesley; 1970.
[16] Serra J. Image analysis and mathematical morphology. New York, London: Academic Press; 1982.
[17] Coster M, Chermant JL. Précis d'analyse d'images. Paris: Les Editions du CNRS, 1985. 2nd ed. Paris: Les Presses du CNRS; 1989.
[18] Chermant JL, Coster M. Granulometry and granulomorphy by image analysis. Acta Stereol 1991;10:7–37.
[19] Chermant JL, Coster M. Analyse de la forme. Acta Stereol 1993;46:45–78.
[20] Cambell DH. Microscopical examination and interpretation of Portland cement and clinker. Portland Cement Association, 1986.
[21] Roux B. Mise au point d'une méthode d'analyse d'images qui reconnaisse et quantifie les phases de clinker. Thèse de Doctorat of the University of Saint-Etienne, 1993.
[22] Roux B, Faure RM. Recognition and quantification of clinker phases by image analysis. In: Proceedings of the Eighth International Congress for Stereology, Irvine, Cf, August 1991. Acta Stereol 1992;11:149–54.
[23] Roux B. Mise au point d'une méthode qui reconnaisse et quantifie les phases de clinker. ATILH, Report No. 4, Paris, 1991.
[24] Lowitz GE. Mapping the local information content of a spatial image. Patt Recogn 1984;17:545–50.
[25] Jourlin M, Pinoli JC. Logarithmic image processing. Acta Stereol 1987;6:651–6.
[26] Zeboudj R. Filtrage, seuillage automatique, contraste et contours du pré-traitement à l'analyse d'image. Thèse de Doctorat of the University of Saint-Etienne, 1988.
[27] Dequiedt AS. Contribution à l'étude morphologique des ciments et bétons par analyse d'images multimodales. Thèse de Doctorat of the University of Caen, 1999.
[28] Dequiedt AS, Vigneron E, Chermant L, Coster M. Etude de l'hydratation d'une pâte de ciment par analyse automatique d'images en microscopie électronique à balayage. Rev Met CIT Sci Génie Mat 2000;97:179–86.
[29] Dequiedt AS, Coster M, Chermant L, Chermant JL. Study of the phase dispersion in concrete by image analysis. Cem Concr Comp 2001;23:215–26.
[30] Dupain R, Lanchon R, Saint-Arroman JC. Granulats, sols et bétons. Paris: Capliez A; 1994.
[31] Redon C. Morphologie et comportement mécanique de bétons renforcés par des fibres de fonte amorphe. Thèse de Doctorat of the University of Caen, 1997.
[32] Redon C, Quenec'h JL, Chermant L, Chermant JL. Influence of superplasticizer and metallic glass ribbons on the macroporosity and the compressive strength in concrete. Acta Stereol 1996;15:233–9.
[33] Mouret M, Bascoul A, Escadeillas G. Study of the degree of hydration of concrete by means of image analysis and chemically bound water. MRS meeting, Boston, December 1996. Adv Cem Based Mater 1997;6:109–15.
[34] Scrivener KL, Pratt PL. The characterization and quantification of cement and concrete microstructures. In: De la Science des matériaux au génie des matériaux. First International Congress of the RILEM, Versailles, France, 7–11 September 1987. London: Chapman and Hall; 1987. p. 61–8.
[35] Copeland LE, Kantro DL. Chemistry of hydration of Portland cement. In: Proceedings of the Fourth International Symposium. Part II: Kinetics of hydration of Portland cement, vol. 43. US Standards Bureau; 1962. p. 443–53.
[36] Dequiedt AS, Coster M, Chermant JL, Jeulin D. Towards a model of concrete mesostructure. Cement Concr Comp 2001;23:289–97.
[37] Hoover KC. Air content and unit weight of hardened concrete. In: Klieger P, Lamond JF, editors. Significance of tests and properties of concrete making materials, vol. 169C. ASTM STP; 1994. p. 296–314.
[38] Power TC. Void spacing as a basis for producing air-entrained concrete. J Amer Concr Inst 1954;50:741–60.
[39] Gagne R, Boisvert A, Pigeon M. Effect of superplasticizer dosage on mechanical properties, permeability and freeze-thaw durability of high-strength concretes with and without silica fume. ACI Mat J 1996;93:111–20.
[40] Redon C, Chermant L, Chermant JL, Quenec'h JL. Characterization of the macroporosity of concrete using automatic image analysis. In: Brandt AM, Li V, Marshall IH, editors. Proceedings of the International Symposium Brittle Matrix Composites, BMC5, Warsaw, 13–15 October 1997. Warsaw: BIGRAF and Woodhead Publishers; 1997. p. 292–9.
[41] Redon C, Chermant L, Coster M, Chermant JL, Quenec'h JL. Sur la mesure de distances inter-bulles dans $\mathbb{R}^2$ par analyse d'images. Bull Lab Ponts & Chaussées 1997;211:25–32.
[42] Dequiedt AS, Redon C, Chermant JL, Chermant L, Coster M. Characterization of diffusion paths of water in concrete by color image analysis. Acta Stereol 1999;18:227–37.
[43] Dequiedt AS, Coster M, Chermant L, Chermant JL. Distances between air-voids in concrete by automatic methods. Cement Concr Comp 2001;23:247–54.
[44] Rosenfield A, Pfaltz JL. Distance functions on digital pictures. Patt Recogn 1968;1:33–61.
[45] Mazars J, Bazant ZP. Cracking and damage: strain localization and size effects. In: Mazars J, Bazant ZP, editors. London, New-York: Elsevier Applied Science; 1989.
[46] Reinhardt HW, Naaman AE. High performance fiber reinforced cement composites. In: Reinhardt HW, Naaman AE, editors. Proceedings of the 15th RILEM and ACI workshop, Mainz, 23–26 June 1991. London, New-York: E & FN Spon, Chapman and Hall; 1992.
[47] Nemati KM, Stroeven P. Fracture analysis of concrete: a stereological approach. In: Proceedings of the Third Conference on Fracture Mechanics of Concrete and Concrete Structures, 12–16 October 1998. Proceedings FRANCOS-3. Freiburg: AEDIFICATIO Publishers; 1998. p. 47–56.
[48] Redon C, Chermant L, Chermant JL, Coster M. A mechanical damage model based on the measurement of microcrack orientation in concrete by Fourier transforms. Acta Stereol 1997;16:287–92.
[49] Redon C, Chermant L, Chermant JL, Coster M. Assessment of fibre orientation in reinforced concrete using Fourier image transform. J Microsc 1998;191:258–65.

[50] Chaix JM, Grillon F. On the rose of directions measurements on the discretized grid of an automatic image analyser. J Microsc 1996;184:208–13.
[51] Debicki G. Contribution à l'étude du rôle de fibres dispersées anisotropiquement dans le mortier de ciment sur les lois de comportement. Les critères de résistance et la fissuration du matériau. Thèse de Doctorat ès Sciences, University of Lyon I, 1988.
[52] Jeulin D. Advances in theory and applications of random sets. In: Jeulin D, editor. Singapore: World Scientific; 1997.
[53] Jeulin D, Villalobos IT, Dubus A. Morphological analysis of UO_2 powder using a dead leaves model. Microsc Microanal Microstruct 1995;6:321–4.
[54] Quenec'h JL, Chermant JL, Coster M, Jeulin D. Example of application of probabilistic models: determination of kinetics parameters during liquid phase sintering. Microsc Microanal Microstruct 1996;7:573–80.
[55] Charollais F, Bauer M, Coster M, Jeulin D, Trotabas M. Modelling the structure of a nuclear ceramic obtained by solid phase sintering. Acta Stereol 1997;16:315–21.
[56] Stroeven M. Discrete numerical modelling of composite materials: application to cementitious materials. PhD Thesis, Technische Universiteit Delft, 1999.
[57] Jeulin D. Modèles morphologiques de structures aléatoires et de changement d'échelle. Thèse de Doctorat ès Sciences Physiques, University of Caen, 1991.